Journal of Computational Physics 382 (2019) 43–60

Contents lists available at ScienceDirect

Journal of Computational Physics

www.elsevier.com/locate/jcp

Optimal observations-based retrieval of topography in 2D shallow water equations using PC-EnKF

Yuepeng Wang [a], Kun Hu [a], Lanlan Ren [a], Guang Lin [b,c,*]

[a] School of Mathematics and Statistics, Nanjing University of Information Science and Technology (NUIST), Nanjing, 210044, China
[b] Department of Mathematics, Purdue University, West Lafayette, IN 47907, USA
[c] School of Mechanical Engineering, Purdue University, West Lafayette, IN 47907, USA

ARTICLE INFO

Article history:
Received 26 July 2018
Received in revised form 25 December 2018
Accepted 7 January 2019
Available online 16 January 2019

Keywords:
Uncertainty quantification
Data assimilation
Polynomial chaos
Ensemble Kalman filter
Optimal design

ABSTRACT

Parameter estimation is an important problem because in many instance uncertain parameters cannot be measured accurately, especially in real-time applications. Information about them is commonly inferred via parameter estimation techniques from available measurements of different aspects of the system response. In this work, we consider the reduction of the uncertain topography parameters of 2D shallow water equations to be inconsistency with the physical observations. This is often quite challenging due to its ill-posed nature of the inverse problem, particularly for the present nonlinear case in high-dimensional random space. We have explored an efficient computational strategy for the solution of the problem in the framework of the polynomial chaos (PC)-based ensemble Kalman filter (PC-EnKF for short). The main idea pursued in this methodology is to introduce a determination of the potential optimal observation location followed by the update of the input topography parameters to be retrieved through the PC-EnKF, wherein the identification of the optimal observation locations is accomplished sequentially via the predictive uncertainty controlled by standard deviation, and then places the corresponding measurement for data assimilation purpose. This is not only to provide more informative measurements but also to improve the topography parameters estimation. The numerical experiments indicate that the optimal observations-based PC-EnKF algorithm is effective in dealing with the current retrieval of topography parameters. It is worth mentioning that an iterative PC-basis rotation technique is particularly useful when attempting to enhance the sparsity and the resulting accuracy. The solution strategy is well suited in the current high-dimensional nonlinear inverse modeling and has shown its appealing potential in the real-world application of complex systems.

1. Introduction

Uncertainty Quantification (UQ) is now an interdisciplinary field of research that has seen rapid growth in the last decades [1,2]. UQ focuses mainly on understanding, quantifying and mitigating uncertainty in computational simulations. Within UQ, a fundamental task is to develop computationally efficient statistical methods by the use of limited and noisy measurement data to make an inference of the input parameters of numerical models of physical systems, reduce the

* Corresponding author at: Department of Mathematics, Purdue University, West Lafayette, IN 47907, USA.
E-mail addresses: eduwyp@nuist.edu.cn (Y. Wang), Guanglin@purdue.edu (G. Lin).

https://doi.org/10.1016/j.jcp.2019.01.004
0021-9991/

corresponding uncertainty and lead to improved models [3,4]. For this reason, the inverse problem has received increased attention.

A rigorous framework for inferring the uncertain input parameters is the Bayesian approach [5], where probability density functions are considered to represent uncertainty. The Bayesian method has been widely used [6]. Different methods to estimate parameters in a Bayesian framework are possible. For example, Maximum likelihood parameter estimation can be formulated as an optimization problem, which can be numerically solved by gradient methods or global optimization methods [7]. Another Bayesian parameter estimation method is the Kalman filter [3].

The Kalman filter is widely used as a data assimilation method. Due to the variety of potential applications of the Kalman filter, there have been several variants of the Kalman filter developed so far. Among them, polynomial chaos based ensemble Kalman filter (PC-EnKF) has recently developed [8–10]. This method overcomes some of the drawbacks of the ensemble Kalman filter (EnKF) [9], and allows representation of non-Gaussian measurement and parameter uncertainties in a simpler, less taxing way without the necessity of managing a large ensemble owing to the use of polynomial chaos.

The PC-EnKF developed by Matthies et al. [10,11] can also be applied to the nonlinear inverse problems. In this method, the random process of interest is represented by the PC bases which are the orthogonal polynomials with respect to a set of independent random variables with known distributions [12,13]. Once the PC representation is obtained, the statistical moments of our interest (i.e. mean and covariance of the random quantities) can be easily computed from the PC coefficients. The PC-EnKF resembles the traditional EnKF in every aspect except that it represents and propagates model uncertainty by PC expansion instead of an ensemble of model realizations. This method turns out to be a more efficient alternative to EnKF for many data assimilation problems [9,14].

In order to determine the unknown PC expansion coefficients of the solution, there commonly exist two types of methods to be resorted to, the intrusive [15–18] and the non-intrusive ones [19–21]. Historically, the intrusive Stochastic Galerkin (SG) method was used in [22]. However, it must solve a system of coupled equations which require robust and efficient solvers and the modification of existing deterministic codes. Often, the form of equations or code used to solve the deterministic equations is complex, which makes the implementation of the intrusive SG method difficult, if not impossible. Compared with the 'intrusive' method, the advantage of 'non-intrusive' method is that there is no need to modify the deterministic solvers for the quantities of interest (QoI). The fundamental idea behind the 'non-intrusive' approach is essentially the repeated application of the existing or legacy deterministic solver. We consider non-intrusive sampling methods in our current study. However, the trade-off is frequently encountered, that is, keeping more PC basis functions in PC decomposition helps to capture uncertainty more accurately, but it increases the computational cost. An ideal PC expansion should accurately represent the model uncertainty but keep the number of basis functions as small as possible. It is challenging to identify such a subset of PC bases that have the strongest impact on the model uncertainty. Recent attempts at extracting only a subset of desired PC bases rely on the compressive sampling [23–26] and the formulation of convex optimization. In this paper, we are more interested in developing a sparsity-promoting PC-EnKF, where a l_1-solver is introduced to determine the coefficients of PC expansion in the prediction step of ensemble Kalman filter.

The l_1-solver essentially combines tools and ideas from convex optimization with compressive sensing. Among the most popular l_1 solvers, the Lasso (least absolute shrinkage and selection operator) [27] has been widely used in compressed sensing and image processing, where many regression coefficients are expected to be zero, and only a small subset of coefficients to be non-zero. The Lasso sparse solution is therefore obtained via a l_1 penalized least-squares criterion. Currently, there are many methods that can be implemented for solving this l_1 optimization problem. For instance, the least angle regression algorithm [28] (achieve the same time complexity as ordinary least-squares regression) and the even more efficient coordinate descent algorithm [29].

However, there are still some of the weaknesses in Lasso estimation, e.g. the Lasso procedure is not stable enough when there exist high correlations among the variables, and Lasso tends to arbitrarily choose some important variables and ignore the other important variables when they have relatively high correlation or group structures [30]. All these often preclude the use and potential advantage of Lasso.

To improve the limitations of the Lasso, we adopt the Bayesian compressed sensing (BCS) method [31]. This method was originated from the area of machine learning and introduced by Tipping for obtaining sparse solutions to regression and classification tasks that use models which are linear in the parameters, coined as relevance vector machine (RVM) [32] or sparse Bayesian learning (SBL). SBL is built upon a statistical perspective where the sparsity information is exploited by assuming a sparsity-inducing prior to the signal of interest that is then estimated via Bayesian inference. Its theoretical performance is analyzed by Wipf and Rao [33]. After being introduced into CS by Ji et al. [31], this technique has become a popular approach to compressed sensing (CS) and other sparsity-related problems. In this paper, we solve the polynomial chaos expansion coefficients with the help of BCS due to its attractive computational efficiency. In contrast to solving the CS problem with l_1 regularization (or l_1 solver), the BCS can, as a significant competitive candidate method, avoid the need to perform the expensive the determination of regularization parameter.

Recently, there are increasing interests in exploring potential observations (future possible observations to be collected). It is desirable to use the smallest set of potential observations to make optimal placement in order to significantly reduce the effort and cost of measurements. There are many methods appear in these areas of optimal measure location. The adjoint sensitivity analysis technique has proven to be an essential tool for developing optimal observation strategies and will be used to help identify the areas where the uncertainties in models are rapidly growing and will mostly influence the forecast. A Bayesian optimization is a powerful tool for the joint optimization of design choices that is gaining great

popularity in recent years [34]. Bayesian optimization has two ingredients that need to be specified: building the prior by adopting the Gaussian process (GP) and searching for the high potential observation location by optimizing the acquisition function. Bayesian optimization methods differ in their choice of prior and their choice of this acquisition function. As an optimization methodology, Bayesian optimization techniques have been successfully applied to environmental monitoring [35], information extraction [36], combinatorial optimization [37], automatic machine learning [38–40], sensor networks [41], adaptive Monte Carlo [42], experimental design [43] and reinforcement learning [44]. Despite many success stories, the GP-based Bayesian optimization approach is beset with potential difficulties and significant challenges, such as high-dimensionality problem [38], and nonlinearity operator [45], which are still the most pressing open question remaining to be dealt with. Based on this consideration, and motivated by the Bayesian optimization we develop the current method in the framework of PC-EnKF and attempt to cope with the retrieval of the topography in 2D shallow water equations. The main idea pursued in this method is to introduce a determination of the potential optimal observation location followed by the update of the input parameters to be retrieved via the PC-EnKF. More details of the description of the algorithm will be seen later in Section 2. We would like to stress that PC-EnKF-based optimal determination for the observation data was rarely studied.

In determining the optimal observation, the main problem is to quantify the impacts of the information content of observed data to be planned on parameter estimation. Different information can be employed in the application. These include the D-optimality, Bayesian D-optimality, Shannon entropy difference, and relative entropy et al. D-optimality maximizes the determinant of the information matrix or equivalently minimizes the variance of estimators, which has been widely used in optimal experimental design theory since late 1950's Kiefer (1959) [46]. As one of the commonly used standard criteria, D-optimality and its main idea have been followed by many researchers [47]. For the current study, we adopted the variance or standard deviation as the control function due to its simplicity and efficiency in computation [45].

The main task of the current work is to explore the feasibility of combining the PC-EnKF with the determination of optimal observation locations when solving the high-dimensional nonlinear inverse problem. And the final purpose is to pursue the desired retrieval effectiveness of the model parameters with a relatively low number of samples and a small number of observations, due to the usage of polynomial chaos and the determination of optimal observation, respectively. Wherein the fast computation of the Kalman gain matrix at the analysis step of EnKF can be guaranteed by the introduction of the Bayesian compressed sensing method that can provide sparse and fast solution results for the polynomial chaos expansion coefficients. For demonstrating the current algorithm, we solve an inverse problem from the 2D shallow water equations and attempt to recover the representation of accurate bed topography that is still a challenge [48,49] due to its ill-posed essence. Such a problem arises frequently in the field of hydraulic modeling of open channel flows in which the topography shape is an important parameter that needs to be identified prior to numerical modeling and flow simulation. So far, various methods have been developed for addressing this issue, please see [50] for details. To the best of our knowledge, the present study is the first development and application of the optimal determination of observation in the theoretical framework of PC-EnKF to deal with the high-dimensional nonlinear inverse problem.

The rest of this paper is organized as follows. First, in Section 2 we provide a formulation of the current algorithm in the framework of the PC-EnKF method; Secondly, in Section 3, numerical simulation experiments are carried out, and the recovery of topography in 2D shallow water equations is allowed to demonstrate the potential benefits and usefulness of the present algorithm, and then some conclusions and ideas in future research are provided in Section 4.

2. A formulation of the current optimal observation algorithm in the framework of the PC-EnKF method

In this section, we give the technical background and the basic approach for the proposed algorithm to find the optimal observation for implementing the desired retrieval of parameters.

2.1. Problem description

The model uncertainty prediction can be described using the following relation:

$$\mathbf{d} = g(\mathbf{m}), \tag{2.1.1}$$

where $\mathbf{m}$ denotes the parametric input variable or input parameter, and $\mathbf{d}$ is the output model uncertainty. Generally, g represents a predictive model. Given a priori knowledge of $\mathbf{m}$, then the corresponding model prediction $\mathbf{d}$ has huge uncertainty. For the purpose of reducing this kind of uncertainty as small as possible, we resort to the observation data from the physical field. Considering the practical measurement error, the observation data $\mathbf{d}^{obs}$ can be written as $\mathbf{d}^{obs} = \mathbf{d} + \epsilon$. Here the ϵ satisfies a certain probability distribution, which is uncorrelated with the prior distribution. So the posterior distribution of $\mathbf{m}$ when considering observation data becomes $P(\mathbf{m}|\mathbf{d}^{obs})$. Thus, the mean value and variance of $\mathbf{m}$ are derived theoretically. In the current study, we will apply the polynomial chaos to express the uncertainties to numerically accomplish the retrieval of the input parameters in the framework of EnKF.

2.2. PC representation of the uncertainty

To characterize uncertainty, we model the uncertain inputs as an n-dimensional vector of independent random variables $\xi := (\xi_1, \xi_2, \cdots, \xi_n)$, with probability density function $\rho(\xi)$. The QoI that we seek to approximate is $\mathbf{d}(\xi)$. Supposed that its variance is finite, then we can utilize PC expansions $\psi_j(\xi)$ to approximate $\mathbf{d}(\xi)$, which is of the form:

$$\mathbf{d}(\xi) = \sum_{j=0}^{P} c_j \psi_j(\xi) + \epsilon_t(\xi), \tag{2.2.1}$$

where c_j, $j = 1, 2, \cdots$, are the corresponding PC expansion coefficients. Denote the maximum order of the truncated polynomials by l, the total number of terms $P+1$ is given by $\frac{(n+l)!}{n!l!}$. ϵ_t is truncation error associated with retaining $P+1$ terms of PC bases. With the growth of the polynomial order and the number of random variables, the total number of terms in the expansion increases rapidly. We assume that $\psi_j(\xi)$ are normalized such that $E(\psi_j^2(\xi)) = 1$, where the operator E denotes the mathematical expectation. In this work, the parametric input variables are assumed to be Gaussian, and therefore Hermite polynomials are chosen according to the Wiener–Askey scheme. The Hermite polynomials are normalized and the weight function is: $w(x) = \frac{1}{\sqrt{2\pi}} \exp(\frac{-x^2}{2})$. To identify PC expansion coefficients, we consider non-intrusive sampling methods, in which deterministic solvers for the QoI are not modified. Such methods include Monte Carlo simulation [51], pseudo-spectral stochastic collocation [52], least squares regression [53], and l_1-minimization [54–57]. The l_1-minimization, as given by the following optimization problem:

$$\tilde{\mathbf{c}} = \arg\min_{\mathbf{c}} \{\|\mathbf{d} - \mathbf{\Psi c}\|_2^2 + \rho \|\mathbf{c}\|_1\}, \tag{2.2.2}$$

has attracted a revived interest and considerable amount of attention in the signal processing literature [58–60] for its sparsity-seeking property, where ρ is the sparse regularization parameter. The problem (2.2.2) can be solved by some heuristic greedy algorithms, e.g. orthogonal matching pursuit (OMP) [61] and least angle regression (LARS) [62]. In light of the high interest in finding more efficient algorithms to solve this problem, many new algorithms have been proposed like the gradient projection (GP) [63], iterative shrinkage-thresholding (IST) [64,65], etc. However, an unavoidable step needs to be introduced at each iteration when solving the problem (2.2.2), that is, determining regularization parameter ρ by adopting the suitable method. Undoubtedly, this will weaken to some extent the computational advantage of the problem (2.2.2) that works for the sparse solution. For this reason, we resort to the Bayesian compressed sensing (BCS) [31] method to approach the polynomial chaos expansion coefficients $\mathbf{c}$. In a Bayesian setting, a full posterior density function is provided, which yields not only the point estimate for the coefficients $\mathbf{c}$ as done by the problem (2.2.2), but also the corresponding uncertainty. More importantly, the BCS becomes a popular approach to compressed sensing (CS) and other sparsity-related problems via the exploitation of an efficient and fast algorithm for its implementation.

Once we have the coefficients of the expansion, we can compute approximate statistics of the output variable $\mathbf{d}$ with the formulas

$$E[\mathbf{d}] = c_0, \tag{2.2.3}$$

$$\mathrm{Var}[\mathbf{d}] = \sum_{j=1}^{P} c_j^2 \left\|\psi_j(\xi)\right\|^2, \quad \text{or} \quad \mathrm{Std}[\mathbf{d}] = \sqrt{\mathrm{Var}[\mathbf{d}]}, \tag{2.2.4}$$

where the $E[\cdot]$, $\mathrm{Var}[\cdot]$, and $\mathrm{Std}[\cdot]$ denote the expectation (or mean), variance and standard deviation, respectively. In the present study, the variance or standard deviation is interesting, which can be used to guide the determination of the optimal observation locations, implemented with the goal of retrieving the topography in the 2D shallow water equations.

2.3. Solving l_1-minimization using BCS

To solve the coefficients $\mathbf{c}$ of the polynomial chaos expansion we will begin with the following relation:

$$\mathbf{d} = \mathbf{\Psi c} + \mathbf{n}, \tag{2.3.1}$$

where $\mathbf{d}$ represents the model output, and $\mathbf{\Psi}$ the basis matrix. $\mathbf{n}$ denotes an error term with the measurement error and truncation error included, which generally satisfies $\mathbf{n} \sim \mathcal{N}(0, \sigma_0^2)$. In the framework of BCS, we aim to find a full posterior density function for $\mathbf{c}$. The BCS is advantageous owing to its seeking-sparsity property and high efficient computation. A brief review is necessary in order to have a fast understanding of the basic idea behind the BCS. For more details, please refer to the literature [31].

(1) The formulation of hierarchical sparseness prior

For coefficient $\mathbf{c}$ to be solved, the following prior is evaluated

$$p(\mathbf{c}|a,b)=\prod_{i=0}^{P}\int_0^{\infty}\mathcal{N}(c_i|0,\alpha_i^{-1})\Gamma(\alpha_i|a,b)\,d\alpha_i, \tag{2.3.2}$$

here the $\boldsymbol{\alpha}=(\alpha_0,\alpha_1,...,\alpha_P)$ can be considered as Gamma prior:

$$p(\boldsymbol{\alpha}|a,b)=\prod_{i=0}^{P}\Gamma(\alpha_i|a,b), \tag{2.3.3}$$

where a and b are the shape and scale parameters of Gamma distribution, respectively. An appropriate choice of the hyperparameters a and b will lead to a sparseness prior as interpreted in [31].

(2) Fast implementation of seeking the hyperparameters

Having the sparseness prior for $\mathbf{c}$ in hand, its posterior can be solved by the relevance vector machine (RVM) [32] with mean and covariance:

$$\boldsymbol{\mu}=\tilde{\alpha}\boldsymbol{\Sigma}\boldsymbol{\Psi}^{\mathbf{T}}\mathbf{d}, \tag{2.3.4}$$

$$\boldsymbol{\Sigma}=(\boldsymbol{\Lambda}+\tilde{\alpha}\boldsymbol{\Psi}^{\boldsymbol{T}}\boldsymbol{\Psi})^{-1}, \tag{2.3.5}$$

where $\tilde{\alpha}=1/\sigma_0^2$, and $\boldsymbol{\Lambda}=\mathbf{diag}(\boldsymbol{\alpha})$. The appropriate treatment of $\boldsymbol{\alpha}$ will play a key role in designing a fast and highly efficient algorithm for coefficients $\mathbf{c}$, which can be formed directly by analyzing the properties of the marginal likelihood function of $\boldsymbol{\alpha},\tilde{\alpha}$ as follows:

$$\mathcal{L}(\boldsymbol{\alpha},\tilde{\alpha})=-\frac{1}{2}[K\log 2\pi+\log|\boldsymbol{C}|+\mathbf{d}^T\boldsymbol{C}^{-1}\mathbf{d}]=\mathcal{L}(\boldsymbol{\alpha}_{-i},\tilde{\alpha})+l(\alpha_i,\tilde{\alpha}), \tag{2.3.6}$$

where $\boldsymbol{C}=\sigma_0^2 I+\boldsymbol{\Psi}\boldsymbol{\Lambda}^{-1}\boldsymbol{\Psi}^T$, K is the number of rows of the matrix $\boldsymbol{\Psi}$, and $l(\alpha_i,\tilde{\alpha})=\frac{1}{2}[\log\alpha_i-\log(\alpha_i+s_i)+\frac{q_i^2}{\alpha_i+s_i}]$. While $s_i=\psi_i^T\boldsymbol{C}_{-i}^{-1}\psi_i$, $q_i=\psi_i^T\boldsymbol{C}_{-i}^{-1}\mathbf{d}$, and $\boldsymbol{C}_{-i}$ is $\boldsymbol{C}$ with the contribution of basis function ψ_i removed. $\boldsymbol{\alpha}_{-i}$ is the same as $\boldsymbol{\alpha}$ except α_i is removed. Obviously, by the $l(\alpha_i,\tilde{\alpha})$, a unique maximum associated with α_i of $\mathcal{L}(\boldsymbol{\alpha},\tilde{\alpha})$ can be found:

$$\alpha_i=\frac{s_i^2}{q_i^2-s_i},\quad q_i^2-s_i>0, \tag{2.3.7}$$

$$\alpha_i=\infty,\quad q_i^2-s_i\le 0. \tag{2.3.8}$$

If $\alpha_i=\infty$ then coefficient $c_i=0$. Controlling in this way the addition and deletion of particular ψ_i from the uncertainty representation guarantees the sparsity of the resulting coefficients, and hence a highly efficient learning algorithm is realized.

2.4. PC-EnKF inverse modeling

Let us go back again to the problem proposed in Section 2.1, where the output variable $\mathbf{d}$ will produce large uncertainty due to the prior distribution of the input parameter $\mathbf{m}$. We want to seek to reduce this uncertainty using the PC-EnKF with the help of the observation data $\mathbf{d}^{obs}$.

The input and output random vectors $\mathbf{m}$ and $\mathbf{d}$ are expressed as two truncated series below:

$$\mathbf{m}\approx\sum_{i=0}^{P}\mathbf{c}_i^{\mathbf{m}}\Psi_i(\xi), \tag{2.4.1}$$

$$\mathbf{d}\approx\sum_{i=0}^{P}\mathbf{c}_i^{\mathbf{d}}\Psi_i(\xi), \tag{2.4.2}$$

where ξ, as stated in Section 2.1, is a random vector comprising a set of independent random variables with given normal distribution. Correspondingly, the $\Psi_i(\xi)$ is the column vector of $\boldsymbol{\Psi}$ that consists of the Hermite PC basis function. PC expansion representation of input parameters (2.4.1) is set according to the prior distribution of $\mathbf{m}$, whereas the coefficients in equation (2.4.2) are obtained by the process mentioned in Section 2.3. For more details about equations (2.4.1) and (2.4.2), please refer to reference [1]. It is also noted that when the correlated input parameters are encountered, the Karhunen–Loève expansion (KLE) can be employed to represent them with uncorrelated random variables. This technique is also known as proper orthogonal decomposition (POD) or, in finite-dimensional setting, principal component analysis (PCA). This situation can be seen later in numerical experiments.

Implementation of PC-ensemble Kalman filter (PC-EnKF) has two steps: the prediction step and update step.

(1) Prediction step

The key idea in the PC expansion technique is to build a polynomial approximation of the forward model response in a same way as in equation (2.4.2). And the PC expansion is used in the PC-EnKF in place of the forward propagation model (2.1.1). Thus, the PC-EnKF prediction step can be performed with the predicted mean $\mu_{\mathbf{d}}$ and covariance matrices $\mathbf{c_{dd}}$ and $\mathbf{c_{dm}}$ as follows:

$$\mu_{\mathbf{d}} = \sum_{i=0}^{P} \mathbf{c_i^d} E(\Psi_i(\xi)) = \mathbf{c_0^d}, \tag{2.4.3}$$

$$\mathbf{C_{dd}} = E((\mathbf{d}-\mu_{\mathbf{d}})(\mathbf{d}-\mu_{\mathbf{d}})^T) = E((\sum_{i=1}^{P} \mathbf{c}_i^{\mathbf{d}} \Psi_i(\xi))(\sum_{j=1}^{P} \mathbf{c}_j^{\mathbf{d}} \Psi_j(\xi))^T) = \sum_{i=1}^{P} \mathbf{c}_i^{\mathbf{d}} \mathbf{c}_i^{\mathbf{d}T}, \tag{2.4.4}$$

$$\mathbf{C_{dm}} = E((\mathbf{d}-\mu_{\mathbf{d}})(\mathbf{m}-\mu_{\mathbf{m}})^T) = E((\sum_{i=1}^{P} \mathbf{c}_i^{\mathbf{d}} \Psi_i(\xi))(\sum_{j=1}^{P} \mathbf{c}_j^{\mathbf{m}} \Psi_j(\xi))^T) = \sum_{i=1}^{P} \mathbf{c}_i^{\mathbf{d}} \mathbf{c}_i^{\mathbf{m}T}, \tag{2.4.5}$$

From these above relations, we see that seeking the sparsity of expansion coefficients indeed facilitates the calculation of statistical moments. Once the prediction stage is finished, then the update step is therefore followed.

(2) Update step

The update step is essentially to correct the PC expansion representation of the parameter vector $\mathbf{m}$ using the Kalman filter once the observations as well as the observation-error covariance matrix $\mathbf{R}$ are given. This can be realized through adopting different Kalman gain matrix that can be fully determined by the statistical moments obtained in the prediction step. When the first coefficient, i.e., the posterior mean of $\mathbf{m}$, is updated, the expression is of the form:

$$\mu_{\mathbf{m}|\mathbf{d}^{\mathbf{obs}}} := \mathbf{c}_0^{\mathbf{m}u} = \mathbf{c}_0^{\mathbf{m}} + \mathbf{K}(\mathbf{d}^{obs} - \mathbf{c}_0^{\mathbf{d}}), \tag{2.4.6}$$

where the superscript 'u' denotes "updated", and the Kalman gain $\mathbf{K}$ is provided by the relations:

$$\mathbf{K} = \mathbf{C_{md}}(\mathbf{C_{dd}} + \mathbf{R})^{-\mathbf{1}}. \tag{2.4.7}$$

While for the coefficients other than the mean (first) term, the update equation becomes:

$$\mathbf{c}_j^{\mathbf{m}u} = \mathbf{c}_j^{\mathbf{m}} - \tilde{\mathbf{K}}\mathbf{c}_j^{\mathbf{d}}. \tag{2.4.8}$$

The corresponding formulation of the Kalman gain is selected as $\tilde{\mathbf{K}}$ in order to guarantee the computational stability [1]:

$$\tilde{\mathbf{K}} = \mathbf{C_{md}}((\mathbf{C_{dd}} + \mathbf{R})^{-1})^T(\sqrt{\mathbf{C_{dd}} + \mathbf{R}} + \sqrt{\mathbf{R}})^{-1}. \tag{2.4.9}$$

Finally, the posterior covariance of the parameters is formed as the following:

$$\mathbf{C_{mm|d^{obs}}} := \sum_{j=1}^{P} (\mathbf{c}_j^{\mathbf{m}u})(\mathbf{c}_j^{\mathbf{m}u})^T, \tag{2.4.10}$$

from which the uncertainty of the resulting input parameters $\mathbf{m}$ can be derived.

2.5. Determination of the optimal observation

Besides immediate access of the gain matrix involved in the ensemble Kalman filter (EnKF), the computation of the coefficients of polynomial chaos expansion, as can be seen from Sections 2.3 to 2.4, will significantly facilitate the determination of the optimal observation. The optimal observations are important as they will allow the most effective use of potential observation resources, which implies a determination where best to place monitoring devices, hence the reduction of inverse solution error as well as assimilation of the fewer observational resource. This approach initially involves the definition of an overall goal (criteria), which is a measure of what is considered important in a physical problem. As mentioned in [45], we adopt variance (or standard deviation) as a criterion, with which an algorithm of determining optimal observation is thus developed here for improving the eventual PC-EnKF result. So the process to identify the optimal observation can be formulated as follows:

$$(x_i^{(k+1)}, y_i^{(k+1)}) = \arg\max_{\boldsymbol{D_{xy}}} \mathrm{Var}^{(k)}(x, y), \tag{2.5.1}$$

where k denotes the k-th PC-EnKF iteration, $(x_i^{(k+1)}, y_i^{(k+1)})$ is the potential observation location where the corresponding observation data will be placed for the assimilation calculation of $(k+1)$-th PC-EnKF iteration, and $\mathrm{Var}(x, y)$ is the predictive variance for a certain output state variable over the numerical computational domain D_{xy}.

Here the predictive variance $\mathrm{Var}^{k+1}(x, y)$ is straightforward to calculate through the equation (2.2.4) once the k-th PC-EnKF is completed. This can be accomplished by evolving the k-th updated input parameters using equation (2.1.1) to the final time of assimilation, and then collecting the relevant coefficients of polynomial chaos expansion. The main steps to perform the current algorithm include:

(1) Stage of preparatory work

a). Generating random vectors $\xi := (\xi_1, \xi_2, \cdots, \xi_n) \sim N(\mathbf{0}, \sigma^2 I_{n\times n})$, where $I_{n\times n}$ is the identity matrix, and σ^2 is a variance;

b). A set of random observation locations, denoted by A, includes n_o elements, and the observation data are correspondingly placed on, represented by $\mathbf{d}_g^{obs}$. It is assumed that the observation error vector $\boldsymbol{\varepsilon}$ follows the Gaussian distribution: $\boldsymbol{\varepsilon} \sim N(\mathbf{0}, \sigma_o^2 I_{n_o\times n_o})$, where σ_0^2 is referred to as the observation-error variance;

c). According to the Gaussian prior information, the input parameter $\mathbf{m}$ can be written as:

$$\mathbf{m} = \sum_{i=0}^{P} \mathbf{c}_i^{\mathrm{m}} \Psi_i(\xi)$$

with the column vector $\Psi_i(\xi)$ of the basis matrix $\boldsymbol{\Psi}$ and its coefficient $\mathbf{c}_i^{\mathrm{m}}$;

(2) The update for both the input parameter $\mathbf{m}$ and the observation data $\mathbf{d}_g^{obs}$

d). Run the numerical model $\mathbf{d} = g(\mathbf{m})$ forward in the framework of the non-intrusive method, and then determine the coefficients $\mathbf{c}_i^{\mathbf{d}}$ of the following expression:

$$\mathbf{d} = \sum_{i=0}^{P} \mathbf{c}_i^{\mathrm{d}} \Psi_i(\xi)$$

$\mathbf{c}_i^{\mathbf{d}}$ consists of two parts: one part is $\mathbf{c}_i^{\mathbf{d}_A}$ that is calculated over the existing observation locations A with BCS for the sake of the sparsity of matrix involved in the Kalman data assimilation; the other part is denoted by $\mathbf{c}_i^{\mathbf{d}_{D_{xy}\setminus A}}$ that can be explored by the least square method when considering the fast calculation of the variance or standard deviation over the other grids $D_{xy}\setminus A$;

e). Calculate the variance at each grid using the equation: $\mathrm{Var} = \sum_{i=1}^{P} (\mathbf{c}_i^d)^2 \|\Psi_i(\xi)\|^2$. If the maximum of variance over the grid domain is lesser than the predefined tolerance δ, then the computational process will be terminated, say after k-th loop, and hence the input parameters $\mathbf{m}^{(k)}$ are just our desired; otherwise placing an observation $d_{\mathbf{v}}^{obs}$ on the position of maximum variance, and add it to the current observation data and form new observation data $\mathbf{d}_{k+1}^{obs} = [\mathbf{d}_k^{obs}, d_{\mathbf{v}}^{obs}]$ to prepare for the $(k+1)$-th data assimilation loop. Meanwhile, proceed to perform the update of the input parameter $\mathbf{m}^{(k)}$ with the observation $\mathbf{d}_k^{obs}$;

f). Use the equations (2.4.3)–(2.4.5) to construct the covariance matrix $\mathbf{C_{dd}}$, $\mathbf{C_{dm}}$. After the Kalman gain $\mathbf{K}$ and $\tilde{\mathbf{K}}$ are computed as stated by the equations (2.4.7) and (2.4.9), the mean and variance of parameters $\mathbf{m}^{(k)}$ can be thus updated using the observation information from $\mathbf{d}_k^{obs}$ according to the equations (2.4.6), (2.4.8) and (2.4.10);

g). Return to the step c) and repeat the above process until the maximum variance of output variable is less than δ. Thus, the input parameters $\mathbf{m}$ are retrieved with the selected observation data $\mathbf{d}^{obs}$.

For the more details, please see Fig. 1. Obviously, this direct evaluation of the standard deviation allows us to avoid any other available optimization algorithm for solving the problem (2.5.1), thus saving the huge computational cost. $\mathrm{Var}(x, y)$ plays an important role in the current study, which acts as not only a tool to measure uncertainty but also a termination criterion for PC-EnKF iteration. This study provides the first application of the algorithm for determining optimal observation in the context of the PC-EnKF for the sake of improving the eventual inverse results.

Remark 2.5.1. For the current study, we adopted the variance or standard deviation as the control function due to the motivation of discrete empirical interpolation method (DEIM) [66], where the selection of indices (spatial locations) is performed according to the largest error found in iteration k and then the next iteration $k+1$ will make the interpolation become as exact as possible at this index (spatial location). This process has something in common with that of the Gaussian process in searching for a measurement helps the most in experimental settings where the model response (or interpolation function) contains the largest uncertainty. In fact, using the location of maximum variance has already been a standard approach in Gaussian process modeling, and has been widely applied in the theoretical study [45].

Remark 2.5.2. When performing the current algorithm, the optimal observation data included in the $\mathbf{d}^{obs}$ are fully replaced with those from the traditional Gaussian process. However, we find from the numerical experiments that the PC-EnKF with

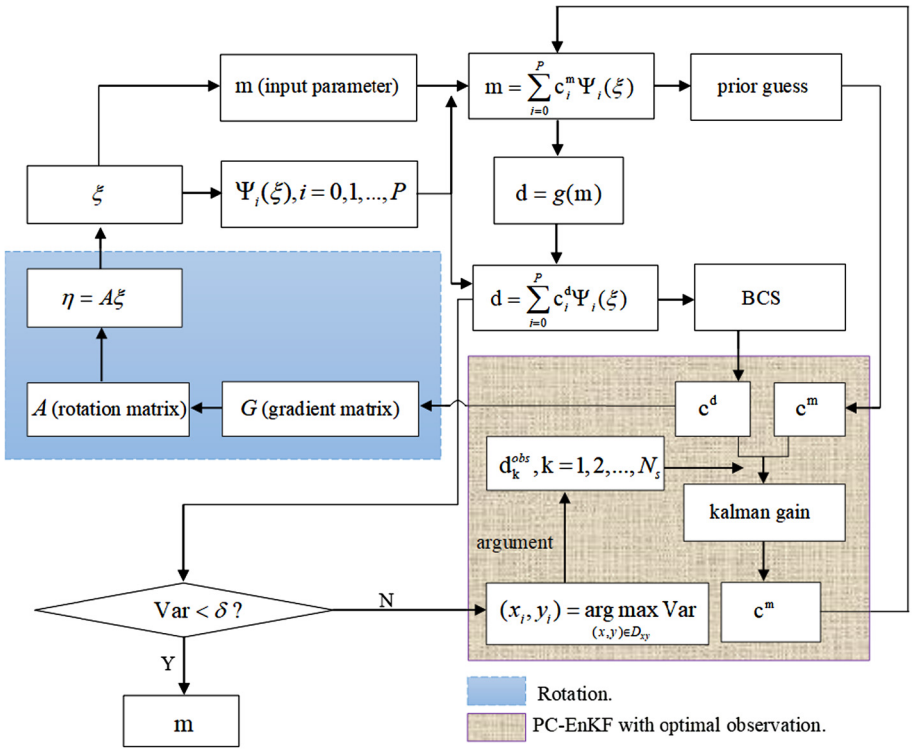

Fig. 1. Flow-chart of the algorithm involved in this paper.

the observation data derived by Gaussian process (PC-EnKF-GP) does not gain too many advantages in computational cost over the PC-EnKF with the present observation data derived by the forecast variance (PC-EnKF-FV), on the contrary, provide the lower the retrieval accuracy of the input parameter **m** than that using the PC-EnKF-FV. In addition, when a very small number of random observation locations are given from the beginning, the Gaussian process can frequently suffer from the choice of the parameters associated with kernel functions, particularly in the higher-dimensionality problem. How to address these issues remains a challenge. Here we completely bypass this hurdle by utilizing the current algorithm developed in this manuscript.

Remark 2.5.3. The alternative advantage of the current algorithm allows the embedment of iterative rotation algorithm [67] to further improve the resulting accuracy, which can be illustrated later in the Section 3.

2.6. Numerical test: the inverse solution of the 2D elliptic PDE with random coefficients

We demonstrate in this subsection the performance (efficiency) of both the PC-EnKF-FV and -GP for the inverse solution of the 2D elliptic PDE with random coefficients.

$$\begin{cases} -\nabla \cdot (a(\mathbf{x},\xi)\nabla u(\mathbf{x},\xi)) = 1, \quad \mathbf{x} \in D, D = [0,1]^2 \\ u(\mathbf{x},\xi) = 0, \mathbf{x} \in \partial D \end{cases}, \tag{2.6.1}$$

where $a(\mathbf{x},\xi)$ represents random coefficient, and $\mathbf{x} = (x, y)$. This equation is of particular interest for studies on uncertainty quantification (UQ) methods.

Assume that $a(\mathbf{x},\xi)$ is unknown beforehand, and can not be directly observed, our objective is to solve it with the help of the observation data of $u(\mathbf{x},\xi)$ so as to reduce resulting uncertainty.

Due to the advantages discussed by Xiu and Karniadakis (2002) [68], Powell and Elman (2008) [69], we use the Karhunen–Loève (KL) type expansion to approximate $a(\mathbf{x},\xi)$ as follows:

$$a(\mathbf{x},\xi) = \mu(\mathbf{x}) + \sum_{i=1}^{N} \sqrt{\gamma_i}\phi_i(\mathbf{x})\xi_i, \tag{2.6.2}$$

where the ξ_i $(i = 1, 2, \cdots, N)$ are independent, identically distributed standard normal random variables, the mean $\mu(\mathbf{x})$ is specified to be zero at each space grid. And N is set to be 10. These leading terms in the KL expansion are retained only by

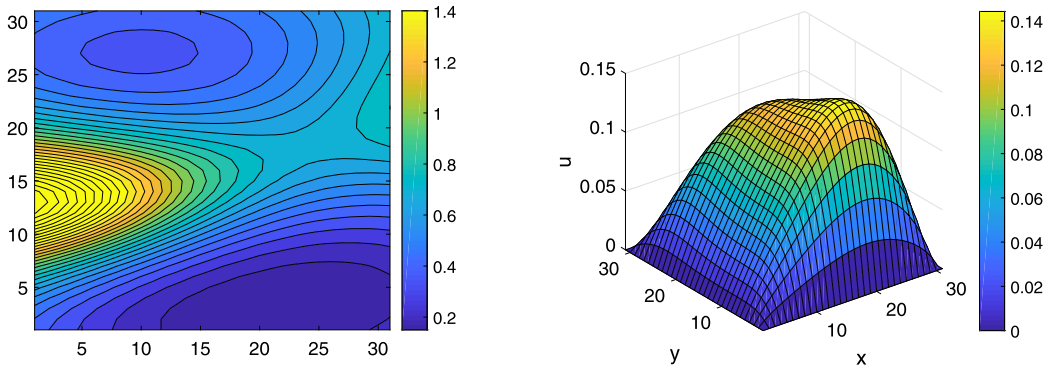

(a) Reference $a(\mathbf{x}, \xi_r)$ (b) Simulation field of $u(\mathbf{x}, \xi_r)$

Fig. 2. The reference of the random coefficient and the corresponding simulation field. (For interpretation of the colors in the figure(s), the reader is referred to the web version of this article.)

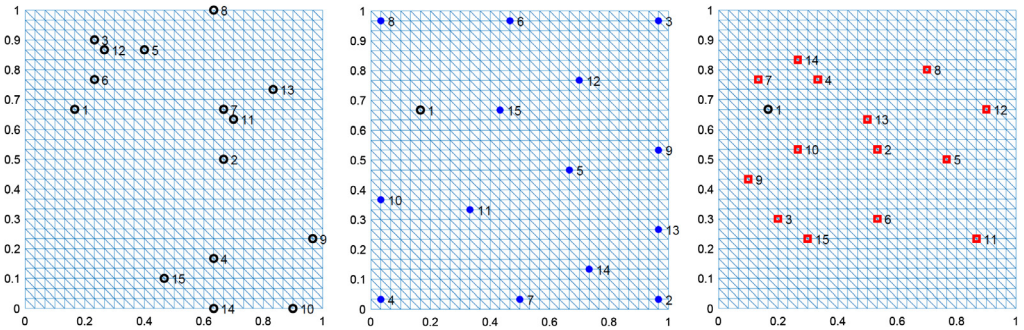

(a) (b) (c)

Fig. 3. The observation locations selected (a) randomly (RD) (denoted by the black circles), (b) by the Gaussian process (GP) (denoted by the blue solid circles) and (c) by forecast variance (FV) (denoted by the red squares). Note that the first location appearing in (b) and (c) is given randomly (see the black circle), respectively.

depending on those that have large variances quantified by the eigenvalues and thus the remaining terms can be dropped from the expansion to yield a reasonable reduced rank approximation of the process. The $\{\sqrt{\gamma_i}, \phi_i\}$ are the eigenpairs of the covariance function:

$$\mathbf{Cov}[a(\mathbf{x}_1), a(\mathbf{x}_2)] = \sigma_a^2 \exp(-\frac{|x_1 - x_2|^2}{l_x^2} - \frac{|y_1 - y_2|^2}{l_y^2}), \tag{2.6.3}$$

where $\sigma_a = 1$ is standard deviation, and the $l_x = 0.3$, $l_y = 0.7$ stand for the correlation length in the x and y direction, respectively. Particularly, one only needs to make an evaluation of the natural exponential function (i.e. nonlinear transform) for equation (2.6.2) if the lognormal distribution of the random coefficient $a(\mathbf{x}, \xi)$ are used on the unit square $D = [0, 1]^2$ in R^2.

Given a reference value $a(\mathbf{x}, \xi_r)$ over the special domain D, see Fig. 2(a), the field simulation $u(\mathbf{x}, \xi_r)$ can be obtained for the same random variable $\xi_r := (\xi_1^r, \xi_2^r, \cdots, \xi_N^r)$ using the standard finite element numerical method, see Fig. 2(b), where we first partition the spatial domain D into squares with mesh size $\Delta x = \Delta y = \frac{1}{30}$, and then further partition them into triangular meshes, please see Fig. 3.

Fig. 3(a), (b) and (c) show us the selected observation locations that are obtained using the random selection, the Gaussian process, and the forecast variance, respectively. Starting with an initial guess $a(\mathbf{x}, \xi_g)$ of the random coefficient (see Fig. 4). We perform the inverse solution by the PC-EnKF with the observations at the locations as shown in Fig. 3. The process of inverse solution is called the PC-EnKF-RD (PC-EnKF with random locations), the PC-EnKF-GP (PC-EnKF with locations determined by the Gaussian process) and the PC-EnKF-FV (PC-EnKF with locations determined by forecast variance), respectively. The inverse results are as follows, see Fig. 5(a), (b), (c).

We can see from the Fig. 5 that the PC-EnKF works well, no matter which kind of the selected observation data is used. All the results have a close approximation to the reference of $a(\mathbf{x}, \xi_r)$, and the substantial improvements are observed. However, for further demonstrating the advantage of the current algorithm, we provide the iterative process of reducing the uncertainty of $a(\mathbf{x}, \xi_g)$ at $x = 12\Delta x$ with the selected observation when performing the PC-EnKF-RD, -GP and -FV data assimilation process, respectively. The corresponding computational results can be shown in Fig. 6. Comparing their

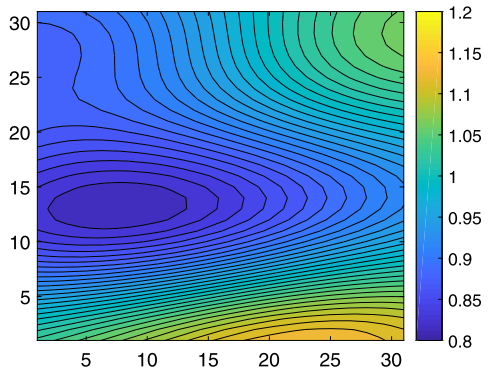

Fig. 4. The initial guess $a(\mathbf{x}, \xi_g)$ of random coefficient.

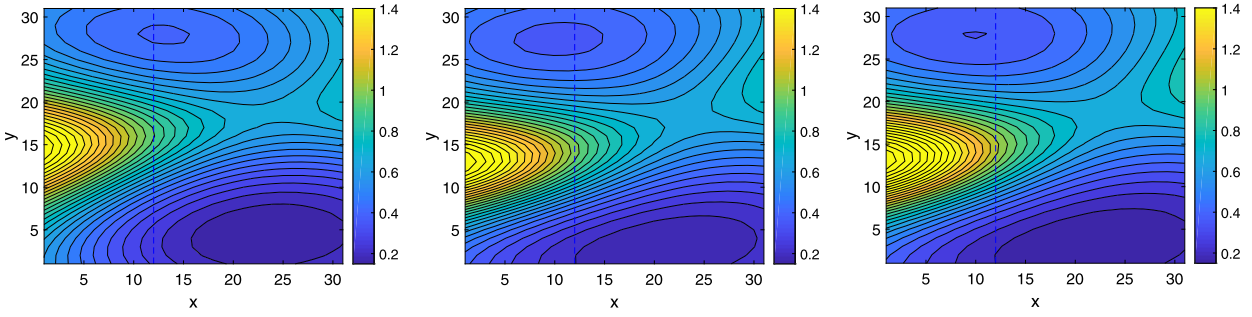

Fig. 5. The inverse results of $a(\mathbf{x}, \xi_g)$ using (a) PC-EnKF-RD, (b) PC-EnKF-GP and (c) PC-EnKF-FV.

final assimilation results (i.e. the fifteenth computational result) we find that the accuracy of the inverse solution of the PC-EnKF-FV is superior to that of other two processes. In fact, in the case of the PC-EnKF-FV, the inverse result that use the thirteen observation data to obtain (i.e., the thirteenth assimilation result) has approached or outperformed the final computational quality for the cases of the PC-EnKF-GP and -RD. In other words, with respect to the same number of observation data the PC-EnKF-FV exhibits a higher convergence order than the PC-EnKF-GP and -RD, which leads us to the retrieval of topography in 2D shallow water equations in Section 3. This is perhaps a more realistic scenario for real world applications, where we will keep the same computational process as in the case of the elliptic equation with random coefficient. However, a more thorough treatment on details that contribute to a better understanding of our algorithm can also be referred there.

3. The recovery of topography in 2D shallow water equations

3.1. Numerical scheme

Numerical experiments will be carried out to demonstrate the efficiency and exactness of the current algorithm, and 2D shallow water equations are selected for this purpose. The shallow water models are extensively used in numerical studies of large-scale atmospheric and oceanic motions. The shallow water equations are a nonlinear hyperbolic system of partial differential equations (conservation laws for depth and momentum) that describe a fluid layer of constant density in which the horizontal scale of the flow is much greater than the layer depth. The dynamics of the single layer model is of course less general than three-dimensional models, but is often preferred because of its mathematical and computational simplicity. The 2D shallow water equations can be written in conservative form as follows:

$$\frac{\partial w}{\partial t} + \frac{\partial (uw + U)}{\partial x} + \frac{\partial (vw + V)}{\partial y} = W, \tag{3.1.1}$$

where $w = (h, uh, vh)^T$ is a vector function, $h(x, y, t)$ is the fluid depth, $u(x, y, t)$ and $v(x, y, t)$ are velocity components in the x and y directions, respectively. $U = (0, gh^2/2, 0)^T$, $V = (0, 0, gh^2/2)^T$, $W = (0, -gh\frac{\partial H}{\partial x}, -gh\frac{\partial H}{\partial y})^T$. "$T$" denotes transpose. g is the gravitational constant, and $H(x, y)$ is the topography. We assume that the spatial domain $\Omega = [-L, L] \times [-D, D]$ is equipped with periodic boundary conditions in the x-direction $(h, u, v)|_{x=-L} = (h, u, v)|_{x=L}$, while in the y-direction, $\frac{\partial u}{\partial y}|_{y=-D} = \frac{\partial u}{\partial y}|_{y=D} = 0$, $v|_{y=-D} = v|_{y=D} = 0$. Initially, $(h, u, v)|_{t=0} = (0.05\exp(-\frac{(x+12)^2}{15} - \frac{y^2}{12}) + 0.2, 0, 0)$.

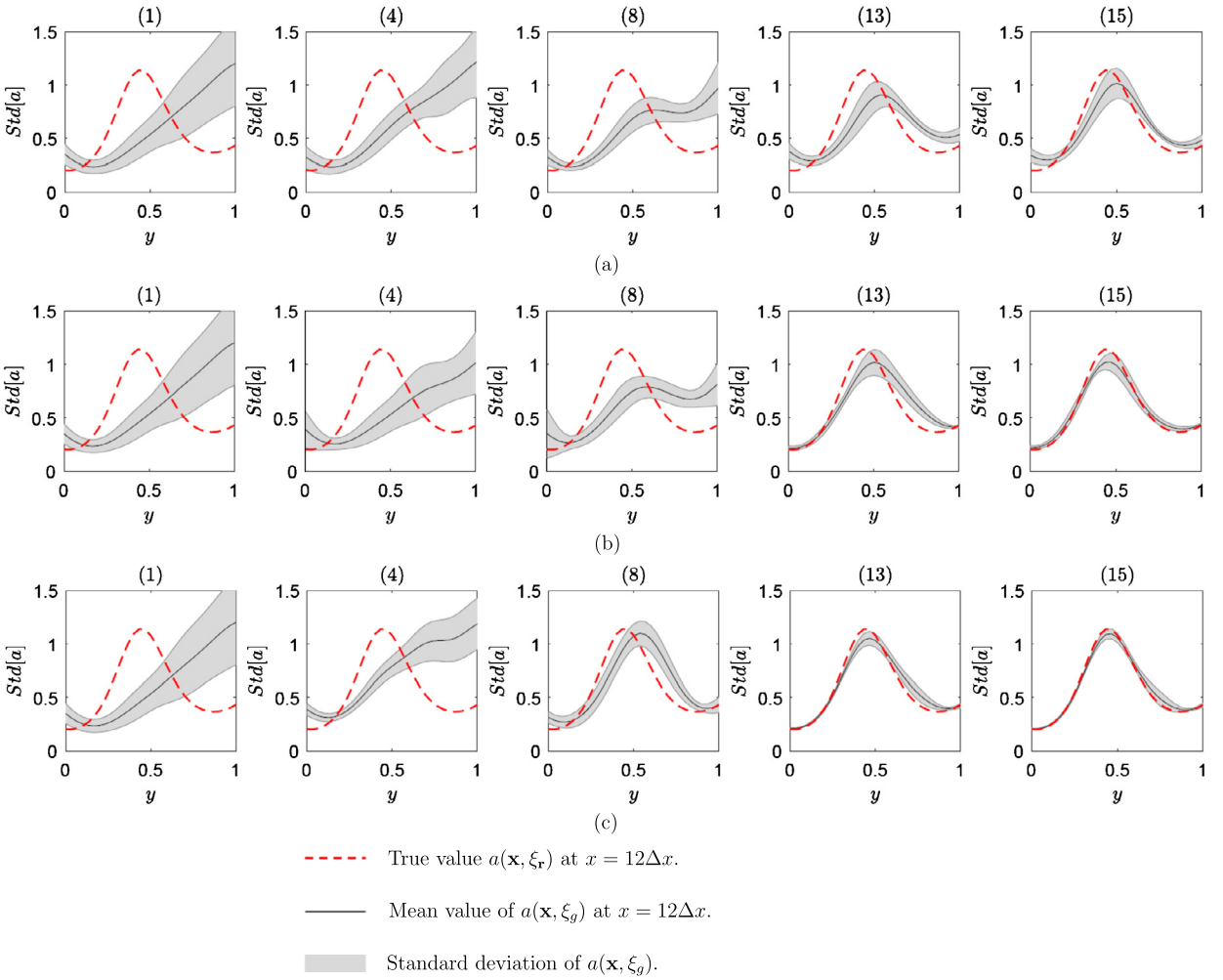

Fig. 6. The reduction process of uncertainty of $a(\mathbf{x}, \xi_g)$ at $x = 12\Delta x$ with the increase of observation data in the case of (a) PC-EnKF-RD, (b) PC-EnKF-GP, (c) PC-EnKF-FV. Note that the number over each subfigure implies the number of observation data used for the current assimilation computation.

Now let us introduce a mesh of $D_{xy} = N_x \cdot N_y$ equidistant points on Ω, with $\triangle x = 2L/(N_x - 1)$, $\triangle y = 2D/(N_y - 1)$. As for the time interval $[0, t_f]$, we discrete it using N_t equally distributed points and $\triangle t = t_f/(N_t - 1)$. Note that it is possible to use adaptive mesh refinement to compute accurate solutions. However, only the uniform mesh is used in this work to avoid coding complications that might be caused by adaptive meshes. Future work will consider an adaptive mesh. Various types of numerical methods have been designed to approximate the solution of the shallow water equations. Methods such as finite volume, finite difference, and discontinuous Galerkin finite element schemes are widely used [70,71]. While in this present study we use the following Lax–Wendroff scheme [72] to integrate the shallow water equation (3.1.1) forward in time

$$w_{i,j}^{n+1} = w_{i,j}^{n} + \triangle t[-\frac{(uw+U)_{i+1/2,j}^{n+1/2} - (uw+U)_{i-1/2,j}^{n+1/2}}{\triangle x} - \frac{(vw+V)_{i,j+1/2}^{n+1/2} - (vw+V)_{i,j-1/2}^{n+1/2}}{\triangle y} + W_{i,j}^{n}], \quad (3.1.2)$$

here $w_{i,j}^{n} := w(x_i, y_j, t_n)$, and $i = 1, 2 \ldots, N_x$, $j = 1, 2, \ldots, N_y$, $n = 1, 2, \ldots, N_t$. The scheme is second-order accurate with respect to both space and time. Unlike the Euler methods which calculate each step of a function, the Lax–Wendroff method involves first calculating a half step and then using the results from the half step to produce the full step (3.1.2). The advantage is that it does not need any artificial diffusion in time or space to keep it stable.

3.2. Uncertainty of input topography

We consider the shallow water equation (3.1.1) with a stochastic topography over the domain $\Omega = [-25, 25] \times [-25, 25]$, and the stochastic topography is unknown and denoted as $H(x, y, \omega)$, $(x, y) \in \Omega$ and $\omega \in \tilde{\Omega}$, where $\tilde{\Omega}$ is a sample space

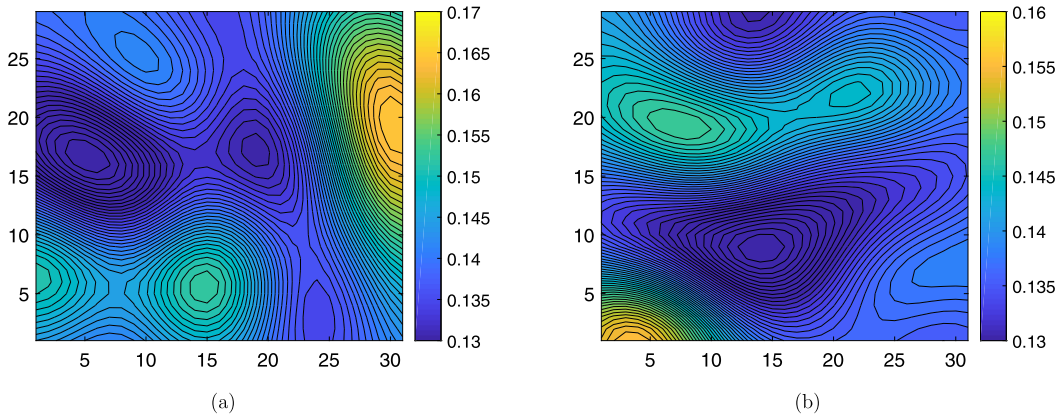

Fig. 7. (a) Reference topography and (b) the initial guess of the topography.

in a probability space $(\tilde{\Omega}, \tilde{U}, \tilde{P})$ with sigma algebra $\tilde{U}$ over $\tilde{\Omega}$, $\tilde{P}$ is a probability measure on $\tilde{U}$. The two-point squared exponential correlation function is commonly used to describe the stochastic fields, and the feasibility has been shown in Subsection 2.6. We assume in the current problem that the stochastic topography field $H(x, y, \omega)$ can be characterized by the following covariance function

$$\mathrm{Cov}_{[H]}(x_1, y_1; x_2, y_2) = \sigma^2 \exp\left(-\frac{|x_1 - x_2|^2}{\lambda_x^2} - \frac{|y_1 - y_2|^2}{\lambda_y^2}\right), \tag{3.2.1}$$

where (x_i, y_i) $(i = 1, 2)$ is the spatial coordinate in 2D. Here $\sigma = 0.1$ is the variance and $\lambda_x = \lambda_y = 12$ are the correlation length in x and y directions. Thus an approximated random topography $H_N(x, y, \omega)$ through a Karhunen–Loève expansion (KLE) truncated at order $N = 20$ is derived, that is,

$$H_N(x, y, \omega) = E[H] + \sum_{i=1}^{N} \sqrt{\lambda_i} b_i \xi_i(\omega), \tag{3.2.2}$$

where $E[\cdot]$ refers to the expectation (i.e., mean over all realizations). The λ_i and b_i are the eigenvalues and orthogonal eigenfunctions of the covariance function (3.2.1). The typical choice of $N = 20$ is that the sum of the neglected terms is sufficiently small compared with the sum of the first N terms. The random vector $\Theta := (\xi_1(\omega), \xi_2(\omega), \cdots, \xi_N(\omega))$ is considered, where ξ_i is mutually independent standard Gaussian random parameter. Thus, the KLE (3.2.2) helps to represent correlated parameters with uncorrelated random variables, which is important from the perspective of dimension reduction of input variables.

Obviously, the input uncertainty in the topography will lead to the uncertainty in the solution of shallow water equations. We will see that a more accurate prediction can be obtained by a less uncertain estimation of the random parameters Θ. This can be done by gathering as more optimal observe information of the output variables as possible to calibrate constantly the simulation results. In this numerical computation, a realization of H as a reference, H_0, is given in Fig. 7(a). The objective of the current inverse problem is to update the input topography given the limited number of observation data only for the fluid height, in the context of 2nd-order Hermite PC expansion, with total $P + 1 = \frac{(20+2)!}{20!2!} = 231$ terms. In order to estimate the PC expansion coefficients for the output variable, a set of samples will be taken. According to the suggestions [73], the number of sample points should be at least twice the number of terms in PCE. However, in our example we conducted several experiments with different numbers of the standard Gaussian sample ensemble members, namely, $N_o = 60$, 100, 200 and 300, respectively. It is eventually shown that adopting only a total sample ensemble size of $N_o = 60$ members was sufficient to successfully perform the current data assimilation algorithm and that using a higher number of ensemble members seems to have no impact on the ensuing results.

When performing the calculation of the PC expansion coefficients, the used BCS package is available online at http://people.ee.duke.edu/~lcarin/BCS.html, for which we make a necessary modification so as to match the present study. Furthermore, if the spatial domain Ω is uniformly discretized into 31×31 grid points, while the time domain $[0, t_f]$ is discretized into 2500 segments, $(t_f = 25)$, a prediction result is then obtained at different times, see Fig. 8.

We are concerned with the case in which the stochastic topography in 2D shallow water equation is unknown a priori to be identified. At this time, an initial guess then needs to be further designated. When the mean of H, according to the equation (3.2.2), is assumed to be $E[H] = 0.14$, along with a realization of the independent standard Gaussian random variables, ξ_i $(i = 1, 2, \cdots, 20)$, an initial topography is therefore derived as in Fig. 7(b). It is easy to find that there is an obvious difference between the Fig. 7(a) and Fig. 7(b), and the uncertainty of initial guess is very large. Without a doubt, the model prediction will be led to have a huge uncertainty. One path to uncertainty reduction of this initial topography is to calibrate the simulation results to available observations on the corresponding quantities (e.g., flow height only in this paper) of the 2D shallow water equations. This task can be completed via the algorithm developed in Section 2.

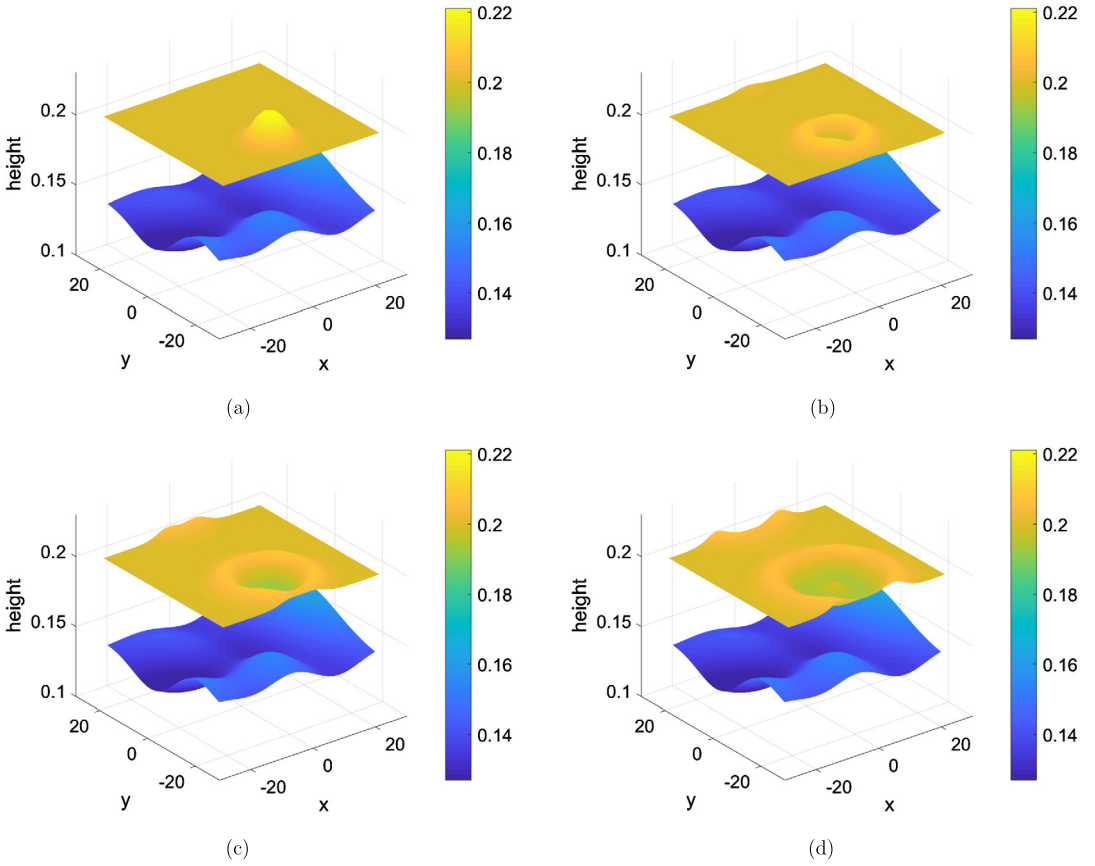

Fig. 8. The height $h(x, y, t, \xi)$ of modeling 2D shallow flow over the topography at time (a) $t = 4$ (top left), (b) $t = 9$ (top right), (c) $t = 14$ (bottom left), (d) $t = 19$ (bottom right), respectively. In each panel, the yellow color is the flow height, and the blue color represents the topography as depicted in Fig. 7(a).

3.3. Reduce the uncertainty of topography using the data placed on the optimal observation locations

It is known generally that the assimilation is required whenever significant flow behavior changes occur. In order to test and sequentially execute our algorithm, a certain number of observation data need to be predefined randomly, besides having an initial guess of topography (see Fig. 7(b)). For clarity, we begin with one observation data that is randomly placed on the computational domain D_{xy} of the fluid height simulated at the final time in the current experiment. Certainly, it can be observed that much more observations data that are randomly placed before starting the PC-EnKF are commonly more favorable for speeding up the computation. Notice that unless stated otherwise, the observation error in our experiment is always set to as $\epsilon_o \sim \mathcal{N}(0, 0.001)$. In our test, the number of the optimal observation location is 23, which are collected in sequential order as can be seen in Fig. 9, where the total number of observation points are up to 24, including the predefined random location.

Intuitively, Fig. 10 shows the behavior of determining the optimal observation location for the next evaluation of the maximal standard deviation over the computational D_{xy}. In Fig. 10, according to the requirement of our algorithm, first given a randomly selected observation location, and starting with the initial guess of topography to carry out the PC-EnKF method, an updated topography is then derived, which can be used for the new evaluation of the maximal standard deviation that implies an alternative potential observation location. Whenever an observation location is determined, the simulated observation data will be rapidly placed at several different time instances $t = 4, 9, 14, 19$, respectively, for the purpose of the PC-EnKF data assimilation. In this way, there are altogether 23 optimal observation locations. Eventually, the desired topography is retrieved. Please note that if an evaluation tolerance is predefined, e.g., $\delta = 0.001$, the whole performing process will be terminated automatically at the 20-th loop, see Fig. 11.

The retrieval result of input topography is presented in Fig. 12(a), which are obtained by the algorithm developed in Section 2. It is easy to see that the resulting recovery of the topography resembles closely the reference topography (see Fig. 7(a)). It can also be observed from Fig. 7(b) that the uncertainty from the initial guess of the stochastic topography has a significant reduction, which confirms in our test example that the optimal observations-based PC-EnKF is feasible and effective.

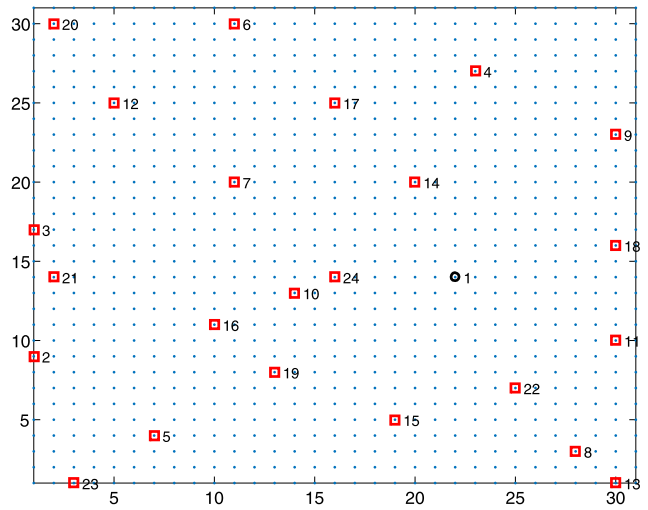

Fig. 9. Observation points of fluid depth. The black circle represents the predefined random observation location (or point), and the red square stands for the optimal observation locations (or points).

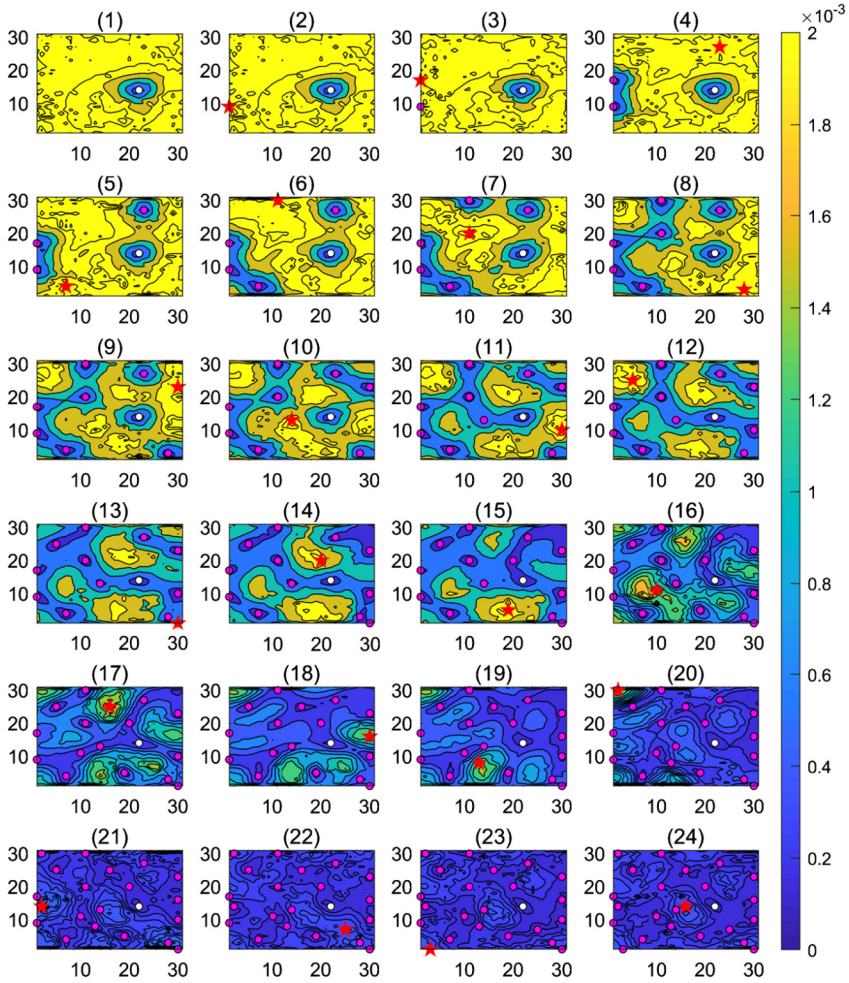

Fig. 10. Illustration of the process for selecting sequentially the optimal observation locations. The first observation location (circle) is given randomly, and the other observation locations are optimally determined (marked by the pink-filled circle). The k-th maximal predictive standard deviation indicates a potential location (denoted as the red star) where the simulated measurement data will be placed for the next update of the topography through the PC-EnKF method, hence the search for the $(k+1)$-th maximal standard deviation. Here $k = 2, 3, \ldots, 24$.

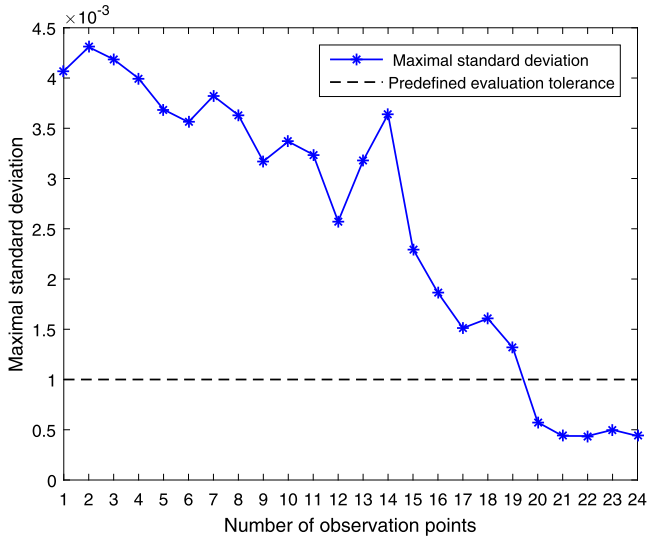

Fig. 11. Evolution of the maximal standard deviation with loops.

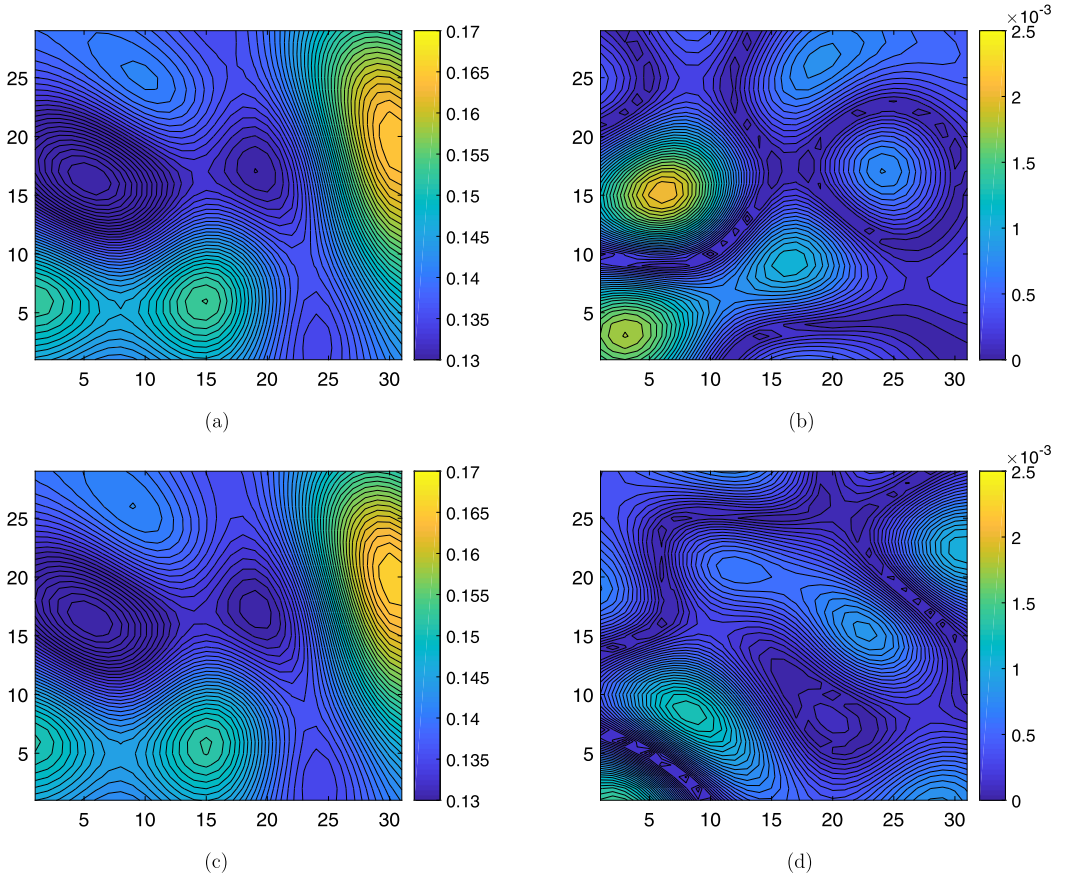

Fig. 12. The retrieval result of topography derived by: (a) the data placed on the optimal observation locations; (c) taking into account the iterative rotation technique based on the case (a). And the corresponding absolute error between the retrieval result and the reference topography are (b) and (d), respectively.

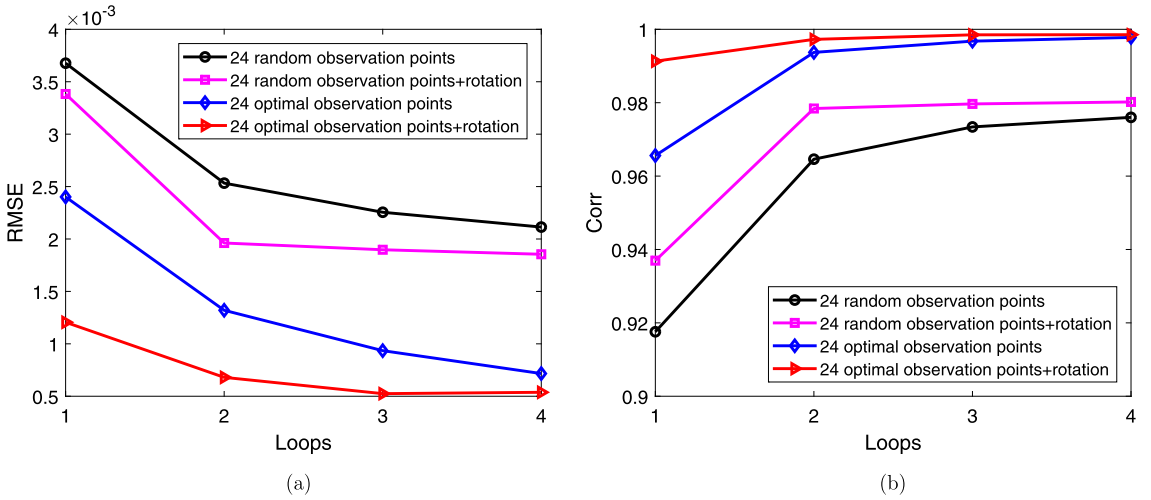

Fig. 13. The variation of **RMSE** (a) and **Corr** (b) with assimilation loop.

If we want to assess how well our retrieval topography approximates the reference topography and see the benefit of our algorithm. Some alternative tools are needed here, such as the root mean square error (**RMSE**) and the correlation coefficients (**Corr**). The computational formulas of the **RMSE** and **Corr** are defined at the assimilation loop k respectively as:

$$\mathbf{RMSE^k} = \sqrt{\frac{\sum_{i=1}^{k_{xy}} (H_i^k - H_{0,i})^2}{k_{xy}}}, \tag{3.3.1}$$

$$\mathbf{Corr(H, H_0)^k} = \frac{E((H^k - E(H))(H_0 - E(H_0)))}{\sigma_{H^k}\sigma_{H_0}}, \tag{3.3.2}$$

where σ_{H^k} is the standard deviation at the k-th data assimilation loop, and k_{xy} represents the number of spatial grids. The variation of **RMSE** and **Corr** with assimilation loop k can be seen from the Fig. 13, and their eventual value approximate to 7.1636e−4 and 0.9978, respectively. These results demonstrate that the accuracy of the inverse solution is satisfying, and illustrate the effectiveness and ability of the current algorithm in dealing with the complex high-dimensional nonlinear inverse problem.

Remark 3.3.1. Despite its advantage in numerical implementation, the current algorithm has still left significant room to further improve the resulting accuracy and performance. For this, we may resort to the newly proposed iterative rotation approach to address this issue. The main idea behind this approach [67] shows that when determining the coefficients of Hermite chaos expansion for QoI of interest, a few of the newly derived coordinates from rotating the original random inputs can have a significant impact on QoI, thereby increasing the sparsity of solution and in turn, the accuracy of recovery. These excellent features exactly cater to the demand of the design algorithm in the framework of PC-EnKF, therefore, are especially suitable for the current study. When we attempt to consider the use of the PC-basis rotation method as is designed in Fig. 1, the resulting accuracy indeed has a considerable improvement, see Fig. 12(c), (d). This can be further found from the computation of **RMSE** and **Corr**, see Fig. 13. This is a first attempt to implement the iterative rotation approach in combination with the optimal observation-based PC-EnKF algorithm when solving the inverse problem. However, the iterative rotation approach is not simple to carry out because there are two key issues to be encountered, for example, the construction of gradient matrix G (see Fig. 1) and the selection of the rotation number etc., for which a more thorough treatment will be involved in another arrangement.

4. Conclusions

In order to retrieve the topography in 2D shallow water equations, we develop an optimal observations-based PC-EnKF method. The main work focuses on the sequential selection of optimal observation locations where the simulated data are placed on for the PC-EnKF data assimilation. The predictive uncertainty controlled by the maximal standard deviation provides a tool to identify the potential locations. A total number of 24 observation locations can meet the retrieval requirement. Besides, when the maximal standard deviation is less than a certain predefined tolerance, say, $\delta = 0.001$, the PC-EnKF assimilation process can be terminated automatically. Thus only 20 observation locations are sufficient for a desired retrieval of topography. In addition, other components involved in designing algorithm also need to be carefully dealt with, for example, adopting the BCS method to cope with the determination of the expansion coefficients of polynomial chaos

for the output uncertainty variable (fluid height). This is advantageous over the l_1-solver because there are no free regularization parameters to be set in sequential computation. The current formulation of the developed algorithm is particularly attractive, for it allows efficient computation via such techniques.

When applying the optimal observation-based PC-EnKF algorithm to reducing the uncertainty of the initial guess of topography in 2D shallow water equations, the corresponding numerical results show that our proposed method is feasible and effective. Meanwhile, the better computation accuracy for the recovery of topography occurs in the case where the PC-EnKF method is coupled with the iterative PC-basis rotation technique. This can be seen from the Fig. 12(c), (d) and Fig. 13. To date, the method has only been developed and tested in the two-dimensional computational models, but the results of this study are extremely positive, which may be viewed as a first step towards solving practical inverse UQ problem by using more realistic observation data and models in order to assess the practical utility of the current method.

In the process of implementing the present algorithm, the non-intrusive sampling method is adopted, which leads to a repeated application of the existing or legacy deterministic solver. It will spend much more time on the large-scale problem, in turn, enhance the computational cost. This may not be an active factor for this method to make a further practical application. However, with the fast development of the reduced-order techniques [66], it is also possible to use the current method in the framework of the inverse problem of the reduced-order model. The associated problem still needs to be further studied in depth as an interesting topic.

Acknowledgement

We thank the anonymous reviewers who contributed in substantially improving the presentation of the manuscript. This work reported here is supported by the National Natural Science Foundation of China (Grant Nos. 41375115, 61572015 and 51728601) and National Science Foundation (DMS-1555072, DMS-1821233, and DMS-1736364).

References

[1] W. Li, G. Lin, D. Zhang, An adaptive ANOVA-based PCKF for high-dimensional nonlinear inverse modeling, J. Comput. Phys. C 258 (2014) 752–772.
[2] H.N. Najm, Uncertainty quantification and polynomial chaos techniques in computational fluid dynamics, Annu. Rev. Fluid Mech. 41 (41) (2009) 35–52.
[3] R.E. Kalman, A new approach to linear filtering and prediction problems, J. Basic Eng. 82 (1960) 35–45.
[4] L. Ljung, Asymptotic behavior of the extended Kalman filter as a parameter estimator for linear systems, IEEE Trans. Autom. Control 24 (1) (2013) 36–50.
[5] B. Thompson, I. Vladimirov, Bayesian parameter estimation and prediction in mean reverting stochastic diffusion models, Nonlinear Anal. 63 (5) (2005) 2367–2375.
[6] J. Wang, N. Zabaras, Using Bayesian statistics in the estimation of heat source in radiation, Int. J. Heat Mass Transf. 48 (1) (2005) 15–29.
[7] J. Nocedal, S.J. Wright, Numerical Optimization, Springer, 2006.
[8] G. Saad, R. Ghanem, Characterization of reservoir simulation models using a polynomial chaos-based ensemble Kalman filter, Water Resour. Res. 45 (4) (2009) 546–550.
[9] J. Li, D. Xiu, A generalized polynomial chaos based ensemble Kalman filter with high accuracy, J. Comput. Phys. 228 (15) (2009) 5454–5469.
[10] O. Pajonk, B.V. Rosić, A. Litvinenko, H.G. Matthies, A deterministic filter for non-Gaussian Bayesian estimation-applications to dynamical system estimation with noisy measurements, Physica D 241 (7) (2012) 775–788.
[11] A. Litvinenko, O. Pajonk, H.G. Matthies, Sampling-free linear Bayesian update of polynomial chaos representations, J. Comput. Phys. 231 (17) (2012) 5761–5787.
[12] D. Xiu, G.E. Karniadakis, Modeling uncertainty in flow simulations via generalized polynomial chaos, J. Comput. Phys. 187 (2003) 137–167.
[13] D. Xiu, G.E. Karniadakis, The Wiener–Askey polynomial chaos for stochastic differential equations, SIAM J. Sci. Comput. 24 (2002) 619–644.
[14] L. Zeng, D. Zhang, A stochastic collocation based Kalman filter for history matching, SPE J. 16 (2) (2011) 294–306.
[15] K. Zhu, X. Lin, K. Li, Compressive sensing and sparse decomposition in precision machining process monitoring: from theory to applications, Mechatronics 31 (2015) 3–15.
[16] Y.M. Marzouk, H.N. Najm, Dimensionality reduction and polynomial chaos acceleration of Bayesian inference in inverse problems, J. Comput. Phys. 228 (6) (2009) 1862–1902.
[17] F. Augustin, A. Gilg, M. Paffrath, Polynomial chaos for the approximation of uncertainties: chances and limits, Eur. J. Appl. Math. 19 (2) (2008) 149–190.
[18] M. Le, O.P. Tre, H.N. Najm, Multi-resolution analysis of Wiener-type uncertainty propagation schemes, J. Comput. Phys. 197 (2) (2004) 502–531.
[19] L. Mathelin, M.Y. Hussaini, T.A. Zang, Stochastic approaches to uncertainty quantification in CFD simulations, Numer. Algorithms 38 (3) (2005) 209–236.
[20] S.S. Isukapalli, A. Roy, P.G. Georgopoulos, Efficient sensitivity/uncertainty analysis using the combined stochastic response surface method and automatic differentiation, Risk Anal. 20 (5) (2000) 591–602.
[21] M.S. Eldred, J. Burkardt, Comparison of non-intrusive polynomial chaos and stochastic collocation methods for uncertainty quantification, in: AIAA Aerospace Sciences Meeting Including the New Horizons Forum and Aerospace Exposition, vol. 976, 2009, pp. 1–20.
[22] I. Babuka, Galerkin finite element approximations of stochastic elliptic partial differential equations, SIAM J. Numer. Anal. 42 (2) (2005) 800–825.
[23] A.M. Bruckstein, D.L. Donoho, M. Elad, From sparse solutions of systems of equations to sparse modeling of signals and images, SIAM Rev. 51 (1) (2009) 34–81.
[24] E.J. Candès, J. Romberg, Errata for quantitative robust uncertainty principles and optimally sparse decompositions, Found. Comput. Math. 7 (4) (2007) 529–531.
[25] E. Candès, J. Romberg, Sparsity and incoherence in compressive sampling, Inverse Probl. 23 (3) (2006) 969–985.
[26] A. Doostan, H. Owhadi, A non-adapted sparse approximation of PDEs with stochastic inputs, J. Comput. Phys. 230 (8) (2011) 3015–3034.
[27] R. Tibshirani, Regression shrinkage and selection via the Lasso, J. R. Stat. Soc. 73 (3) (2011) 267–288.
[28] B. Efron, T. Hastie, I. Johnstone, Least angle regression, Ann. Stat. 32 (2) (2004) 407–451.
[29] W. Wang, B. Zhang, Adaptive sampling with Bayesian compressive sensing in radar sensor networks and image, EURASIP J. Wirel. Commun. Netw. 2012 (1) (2012) 257.
[30] N. Xiao, Q.S. Xu, Multi-step adaptive elastic-net: reducing false positives in highdimensional variable selection, J. Stat. Comput. Simul. 85 (18) (2015) 3755–3765.
[31] S. Ji, Y. Xue, L. Carin, Bayesian compressive sensing, IEEE Trans. Signal Process. 56 (6) (2008) 2346–2356.

[32] M.E. Tipping, A. Smola, Sparse Bayesian learning and the relevance vector machine, J. Mach. Learn. Res. 1 (3) (2001) 211–244.
[33] D.P. Wipf, B.D. Rao, Sparse Bayesian learning for basis selection, IEEE Trans. Signal Process. 52 (8) (2004) 2153–2164.
[34] B. Shahriari, K. Swersky, Z. Wang, Taking the human out of the loop: a review of Bayesian optimization, Proc. IEEE 104 (1) (2015) 148–175.
[35] R. Marchant, F. Ramos, Bayesian optimisation for intelligent environmental monitoring, in: IEEE International Conference on Intelligent Robots and Systems, 2012, pp. 2242–2249.
[36] Z. Wang, B. Shakibi, L. Jin, Bayesian multi-scale optimistic optimization, Eprint Arxiv, 2014, 1005–1014.
[37] F. Hutter, H.H. Hoos, K. Leyton-Brown, Sequential model-based optimization for general algorithm configuration, in: Learning and Intelligent Optimization, Springer, Berlin, Heidelberg, 2011, pp. 507–523.
[38] J. Snoek, H. Larochelle, R.P. Adams, Practical Bayesian optimization of machine learning algorithms, in: International Conference on Neural Information Processing Systems, Curran Associates Inc., 2012, pp. 2951–2959.
[39] K. Swersky, J. Snoek, R.P. Adams, Multi-task Bayesian optimization, Adv. Neural Inf. Process. Syst. (2013) 2004–2012.
[40] M.D. Hoffman, B. Shahriari, N.D. Freitas, On correlation and budget constraints in model-based bandit optimization with application to automatic machine learning, in: Artificial Intelligence and Statistics, 2014, pp. 365–374.
[41] N. Srinivas, A. Krause, S.M. Kakade, Gaussian process optimization in the bandit setting: no regret and experimental design, Eprint Arxiv 58 (5) (2009) 1015–1022.
[42] N. Mahendran, Z. Wang, F. Hamze, N.D. Freitas, Adaptive MCMC with Bayesian optimization, J. Mach. Learn. Res. 22 (2012) 751–760.
[43] J. Azimi, A. Jalali, X. Fern, Hybrid batch Bayesian optimization, in: International Conference on Machine Learning, 2012.
[44] E. Brochu, V.M. Cora, N.D. Freitas, A tutorial on Bayesian optimization of expensive cost functions with application to active user modeling and hierarchical reinforcement learning, Comput. Sci. (2010).
[45] M. Raissi, P. Perdikaris, G.E. Karniadakis, Inferring solutions of differential equations using noisy multi-fidelity data, J. Comput. Phys. 335 (2017) 736–746.
[46] J. Kiefer, Optimum experimental designs, J. R. Stat. Soc. 21 (2) (1959) 272–319.
[47] W. Nowak, F.P.J.D. Barros, Y. Rubin, Bayesian geostatistical design: task-driven optimal site investigation when the geostatistical model is uncertain, Water Resour. Res. 46 (3) (2010) 374–381.
[48] R.C. Hilldale, D. Raff, Assessing the ability of airborne LiDAR to map river bathymetry, Earth Surf. Process. Landf. 33 (5) (2008) 773–783.
[49] R.M. Westaway, S.N. Lane, D.M. Hicks, The development of an automated correction procedure for digital photogrammetry for the study of wide, shallow, gravel-bed rivers, Earth Surf. Process. Landf. 25 (2) (2015) 209–225.
[50] A.F. Gessese, M. Sellier, E. Van Houten, G. Smart, Reconstruction of river bed topography from free surface data using a direct numerical approach in one-dimensional shallow water flow, Inverse Probl. 27 (2) (2011) 025001.
[51] M.T. Reagan, H.N. Najm, R.G. Ghanem, O.M. Knio, Uncertainty quantification in reacting-flow simulations through non-intrusive spectral projection, Combust. Flame 132 (3) (2003) 545–555.
[52] P.G. Constantine, M. Eldred, E. Phipps, Sparse pseudospectral approximation method, Comput. Methods Appl. Mech. Eng. 229 (3) (2012) 1–12.
[53] G. Migliorati, F. Nobile, E.V. Schwerin, R. Tempone, Approximation of quantities of interest in stochastic PDEs by the random discrete L^2 projection on polynomial spaces, SIAM J. Sci. Comput. 35 (3) (2013) A1440–A1460.
[54] P. Ji, J. Hampton, A. Doostan, A weighted l_1-minimization approach for sparse polynomial chaos expansions, J. Comput. Phys. 267 (5) (2014) 92–111.
[55] L. Yan, L. Guo, Stochastic collocation algorithms using l_1-minimization for Bayesian solution of inverse problems, SIAM J. Sci. Comput. 37 (3) (2015) 1410–1435.
[56] X. Yang, G.E. Karniadakis, Reweighted l_1 minimization method for stochastic elliptic differential equations, J. Comput. Phys. 248 (2013) 87–108.
[57] J.D. Jakeman, M.S. Eldred, K. Sargsyan, Enhancing l_1-minimization estimates of polynomial chaos expansions using basis selection, J. Comput. Phys. 289 (C) (2015) 18–34.
[58] D. Baron, M.B. Wakin, M.F. Duarte, Distributed compressed sensing, Preprint, 2005, 22 (10), 2729–2732.
[59] A.M. Bruckstein, D.L. Donoho, M. Elad, From sparse solutions of systems of equations to sparse modeling of signals and images, SIAM Rev. 51 (1) (2009) 34–81.
[60] A.Y. Yang, M. Gastpar, R. Bajcsy, Distributed sensor perception via sparse representation, Proc. IEEE 98 (6) (2011) 1077–1088.
[61] G. Davis, S. Mallat, M. Avellaneda, Adaptive greedy approximations, Constr. Approx. 13 (1) (1997) 57–98.
[62] B. Efron, T. Hastie, I. Johnstone, R. Tibshirani, Least angle regression, Ann. Stat. 32 (2) (2004) 407–451.
[63] M.A.T. Figueiredo, R.D. Nowak, S.J. Wright, Gradient projection for sparse reconstruction: application to compressed sensing and other inverse problems, IEEE J. Sel. Top. Signal Process. 1 (4) (2008) 586–597.
[64] I. Daubechies, M. Defrise, C.D. Mol, An iterative thresholding algorithm for linear inverse problems with a sparsity constraint, Commun. Pure Appl. Math. 57 (11) (2010) 1413–1457.
[65] S.J. Wright, R.D. Nowak, M.A.T. Figueiredo, Sparse reconstruction by separable approximation, IEEE Trans. Signal Process. 57 (7) (2009) 2479–2493.
[66] Y.P. Wang, I.M. Navon, X.Y. Wang, Y. Cheng, 2D Burgers equation with large Reynolds number using POD/DEIM and calibration, Int. J. Numer. Methods Fluids 82 (12) (2016) 909–931.
[67] X. Yang, H. Lei, N.A. Baker, G. Lin, Enhancing sparsity of Hermite polynomial expansions by iterative rotations, J. Comput. Phys. 307 (C) (2016) 94–109.
[68] D.B. Xiu, G.E. Karniadakis, Modeling uncertainty in steady state diffusion problems via generalized polynomial chaos, Comput. Methods Appl. Mech. Eng. 191 (43) (2002) 4927–4948.
[69] C.E. Powell, H.C. Elman, Block-diagonal preconditioning for spectral stochastic finite-element systems, IMA J. Numer. Anal. 29 (2) (2008) 350–375.
[70] R.J. LeVeque, D.L. George, M.J. Berger, Tsunami modeling with adaptively refined finite volume methods, Acta Numer. 20 (20) (2011) 211–289.
[71] A. Duran, F. Marche, Recent advances on the discontinuous Galerkin method for shallow water equations with topography source terms, Comput. Fluids 101 (2014) 88–104.
[72] T. Heuzé, Lax–Wendroff and TVD finite volume methods for unidimensional thermomechanical numerical simulations of impacts on elastic–plastic solids, J. Comput. Phys. 346 (2017) 369–388.
[73] S. Hosder, R.W. Walters, M. Balch, Efficient sampling for non-intrusive polynomial chaos applications with multiple uncertain input variables, in: AIAA Non-Deterministic Approaches Conference, vol. 4, 2007, pp. 23–26.